Hindawi
Advances in Materials Science and Engineering
Volume 2018, Article ID 3071495, 8 pages
https://doi.org/10.1155/2018/3071495

Research Article

Influence of Deformation Conditions on the Critical Damage Factor of AZ31 Magnesium Alloy

Li-juan Pang,[1] Xin Shang,[2] and Xuefeng Zhang[1]

[1]*Panzhihua University, Panzhihua 617000, China*
[2]*Dongguan University of Technology, Dongguan 523808, China*

Correspondence should be addressed to Xuefeng Zhang; wzyzxf@126.com

Received 31 October 2017; Revised 1 April 2018; Accepted 21 May 2018; Published 27 June 2018

Academic Editor: Fantao Kong

The influence of deformation conditions on the critical damage factor of AZ31 magnesium alloy was analyzed in this paper. Physical experiments and numerical simulation were used to study the critical damage factor. Compression test was carried out using a Gleeble 1500 device at temperatures between 250°C and 400°C, as well as strain rates from 0.01 s^{-1} to 1 s^{-1}. True stress-strain curves of samples were obtained. Based on experimental data, an Arrhenius constitutive model was constructed. Material performance parameters and constitutive model were inputted into the finite element program DEFORM. Simulation results show that the maximum damage appears on the outer edge of the upsetting drum, and damage softening behavior is more sensitive to strain rate. According to the concept of damage sensitive rate, its values were computed. The intersection of line fitted and horizontal axis was obtained in the fracture step, and its relative maximum damage value was as the critical damage factor. The distribution of the critical damage value shows that it is not a constant but fluctuates within the range of 0.1445–0.3759, and it is more sensitive to strain rate compared with temperature.

1. Introduction

Magnesium alloys are widely used in many industrial sectors because of their good mechanical properties, high strength to weight ratio, and good formability compared with other metallic alloys. However, these alloys have limited workability at room temperature owing to insufficient slip systems. Thus, bulk forming, such as extrusion, forging, and rolling, is usually conducted at high temperature, where additional slip systems are activated [1–7]. The emergence of ductile fracture in many metal forming processes is a restriction factor [8, 9]. Metal material toughness damage occurs when materials in plastic deformation have a fracture tendency of physical quantity, especially when damage is up to the critical value, or when the material is broken [10]. At present, few local and foreign studies have focused on the critical damage factor by material effects of shape conditions [11–13]. In the process of studying the critical damage factor, the Cockroft–Lathem is widely used to predict the crackle in volume forming [14, 15]. Some scholars believe that critical damage factors are related to material metallurgical properties and cannot change with the deformation process conditions. Besides, the constitutive model plays an important role in hot forming process which is helpful to choose hot deformation parameters and forming forces. At the same time, it is the premise for the plastic forming process which is used for numerical simulation software.

The present work aimed at material high-temperature flow stress performance by a Gleeble 1500 thermomechanical simulator. Based on experimental data, a constitutive model of flow stress was built and used to improve operation accuracy. Some scholars have previously imported the true stress-strain into software, but some errors exist in the operation process because experimental data fluctuate heavily. In this research, material performance parameters and high-temperature constitutive model were inputted into DEFORM to study the critical damage factors. And the maximum damage values were regarded as the critical damage factors. Thus, the law of the critical damage factor was obtained at temperatures between 250 and 400°C as well

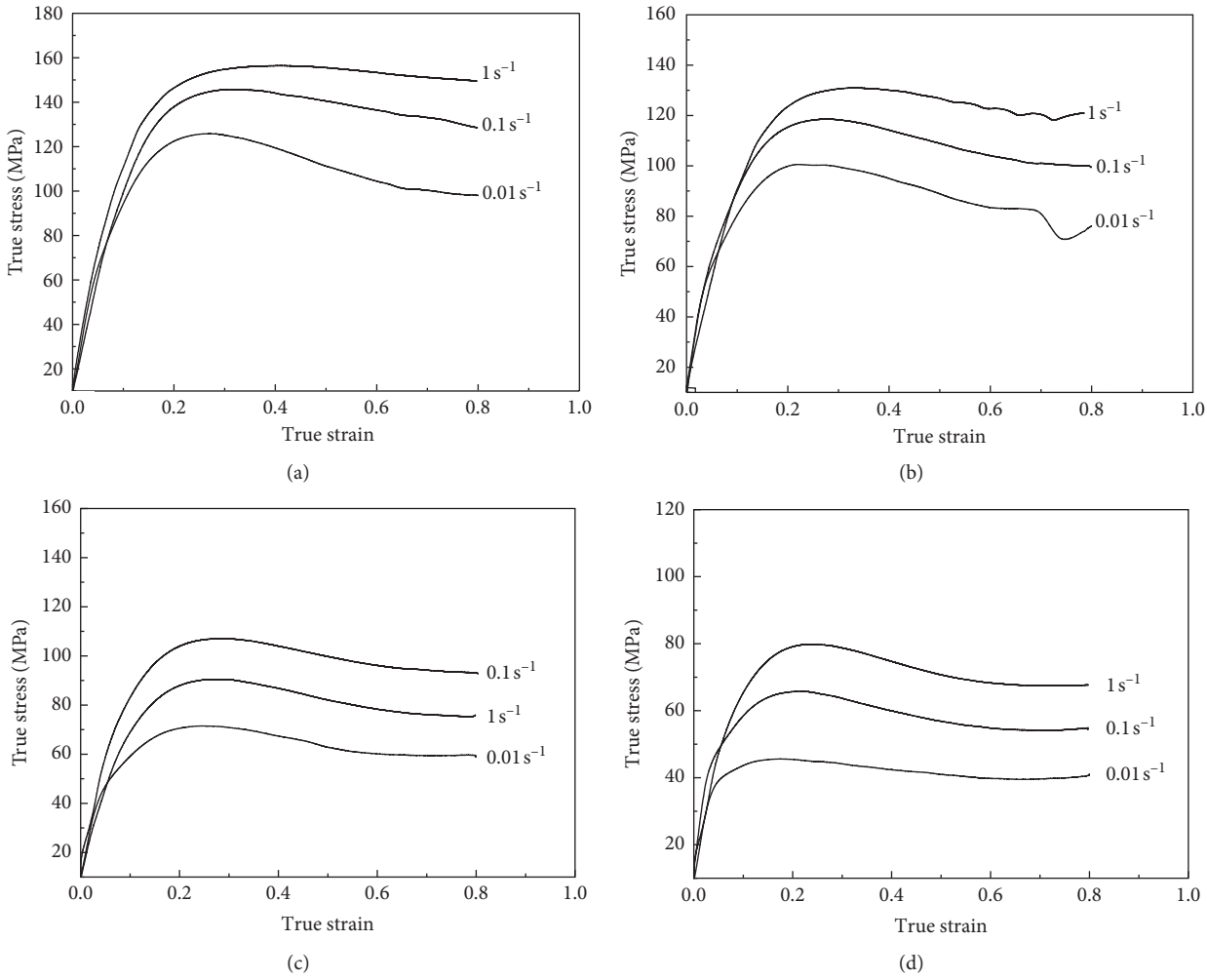

Figure 1: True stress-strain curves of AZ31 at varied temperatures: (a) 250°C; (b) 300°C; (c) 350°C; (d) 400°C.

as strain rates between 0.01 and 1 s^{-1}. Hot forming processes were also controlled and optimized to avoid some defects.

2. Experiments

AZ31 magnesium alloys were used in the experiment. AZ31 magnesium alloy ingots (chemical composition (wt.%): 2.94% Al; 0.87% Zn; 0.57% Mn; 0.0027% Fe; 0.00112% Si; 0.0008% Cu; 0.0005% Ni; and balance Mg) were cut from cylindrical ingots with a diameter of 10 mm and length of 12 mm, and 12 samples were prepared for testing in all. The high-temperature flow stress test was carried out using a Gleeble 1500 machine to obtain stress-strain data at different temperatures. Magnesium alloy is as cast. All the samples were subjected to rapid water quenching at a temperature of 400°C for 12 hours. The height to diameter ratios of specimens are generally less than 1.5, so the impact on the one-way compressive strength is the smallest.

Conditions for isothermal uniaxial compression were as follows: strain rates from 0.01 s^{-1} to 1 s^{-1} and temperatures from 250°C to 400°C. Gleeble 1500 was used to achieve constant true strain rates during compression. The maximum deformation degree was 60%. Graphite powder mixed with grease was used as lubricant in all experiments. Specimens deformed up to a true strain and then quenched in water. Load-stroke data were converted into true stress-true strain curves using standard equations. A specimen was heated quickly at the heating rate of 1°C·s^{-1} to deformation temperature, and holding time was set to 5 min to reduce and eliminate the temperature gradient within the specimen.

3. Results and Discussion

The true strain-stress curves at 250, 300, 350, and 400°C for different strain rates are shown in Figures 1(a)–1(d), respectively. Flow stress increases when decreasing temperature or increasing strain rate. With true strain increasing, true stress gets to the maximum value because of work hardening mechanism, and at this stage, dynamic recovery and recrystallization just take place in some parts of magnesium alloy.

Dynamic recrystallization is believed to be responsible for flow-softening behavior because it involves the nucleation of grains in the initial stages of deformation followed by grain-boundary migration. When a steady state is reached, the rates of nucleation and migration balance each

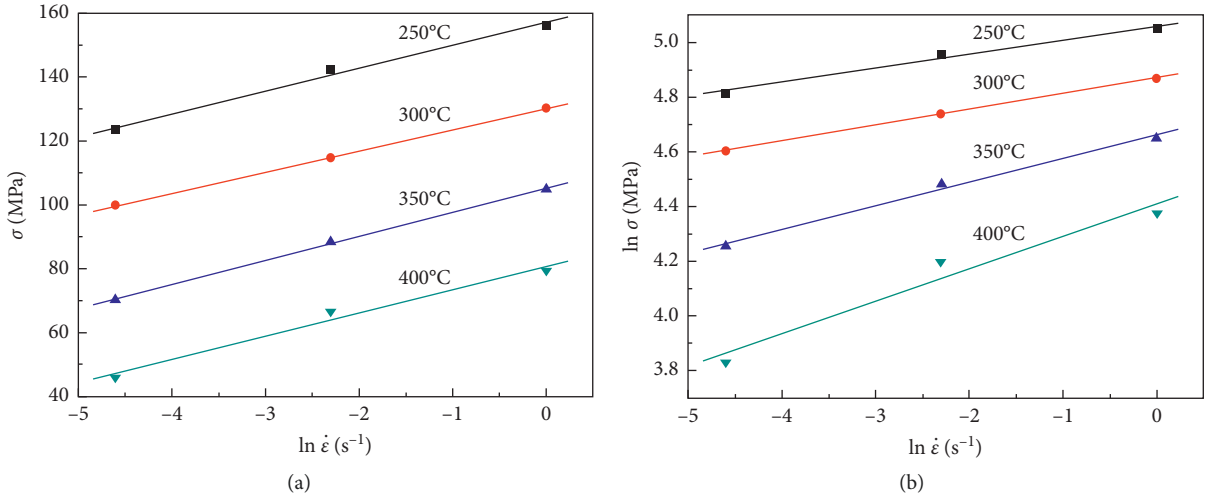

FIGURE 2: Curves of peak stress versus strain rate and temperature under different conditions: (a) $\sigma - \ln \dot{\varepsilon}$; (b) $\ln \sigma - \ln \dot{\varepsilon}$.

other, and the effect of any difference in the initial microstructure is wiped out [16]. Besides, the true strain-stress curves are not smooth curves but thin zigzag curves. Mutual competition between dynamic recrystallization and hot work hardening results in strengthening and softening interaction.

3.1. Construction of Constitutive Model. Flow strain and flow stress depend on the heating temperature of materials which can be inducted from the true stress-strain curve. Meanwhile, these above parameters are related to material performance virtually. Especially, metal high deformation is a process of thermal activation, and deformation temperature and strain rate affect flow stress which is expressed by the Arrhenius equation. Based on experimental data, a high-temperature constitutive model was built with Arrhenius model theory [17–19]:

$$\dot{\varepsilon} = A[\sin h(\alpha\sigma)]^n \exp\left[\frac{-Q}{RT}\right], \tag{1}$$

where σ, $\dot{\varepsilon}$, and Q are stress rate, strain rate, and deformation activation energy, respectively. K, n, and R represent absolute temperature, stress exponent, and molar gas constant; α and A are constants related to material performance.

The hyperbolic sine model ($\sin h(x) = (e^x - e^{-x})/2$) of Thaler was expressed as follows:

$$\sin h(x) = \frac{e^x - e^{-x}}{2} = x + \frac{x^3}{3!} + \frac{x^5}{5!} + \frac{x^7}{7!} + \cdots. \tag{2}$$

At $x < 0.8$, the above trinomial item is negligible, so $\sin h(x) \approx x$, and the relative error <4.2%. At $x > 1.2$, e^{-x} item is negligible, so $\sin h(x) \approx e^{-x}/2$, and the relative error is less than 1.9%. Thus, the Arrhenius equation of $\sin h(x)$ can be simplified as a linear or exponential function as follows:

$$\dot{\varepsilon} = A_1 \sigma^n \exp\left(\frac{-Q}{RT}\right), \qquad (\alpha\sigma \le 0.8), \tag{3}$$

$$\dot{\varepsilon} = A_2 \exp(\beta\alpha) \exp\left(\frac{-Q}{RT}\right), \qquad (\alpha\sigma \ge 1.2), \tag{4}$$

$$\dot{\varepsilon} = A[\sin h(\alpha\sigma)]^n \exp\left[\frac{-Q}{RT}\right], \qquad (\alpha\sigma \text{ is arbitary value}), \tag{5}$$

where A_1, sA_2, and β are expressed as $A_1 = A\sigma n_1$, $A_2 = (A/2)n_1$, and $\beta = \alpha n_1$, respectively.

Because the four parameters Q, R, T, and A are constant, the logarithm of both sides of formulas (3) and (4) can be taken:

$$\ln \dot{\varepsilon} = B_1 + n_1 \ln \sigma, \tag{6}$$

where B_1 is equal to $\ln A_1 - (Q/RT)$, and

$$\ln \dot{\varepsilon} = B_2 + \beta\sigma, \tag{7}$$

where B_2 is equal to $\ln A_1 - (Q/RT)$. Finally, n_1 and β are confirmed, that is, $n_1 = \partial \ln \dot{\varepsilon}/\partial \ln \sigma$ and $\beta = \partial \ln \dot{\varepsilon}/\partial\sigma$.

The peak stress values under different conditions were regarded as strain-stress, and the relationship curves of $\sigma - \ln \dot{\varepsilon}$ and $\ln \sigma - \ln \dot{\varepsilon}$ were fitted, as showed in Figure 2.

As shown in Figure 2(a), n_1 is obtained by the linear slope reciprocal of the mean value, that is, $n_1 = 7.101$. As shown in Figure 2(b), β is obtained by the linear slope reciprocal of the mean value, that is, $\beta = 0.0785$. So, $\alpha = \beta/n_1 = 0.0111\ \text{MPa}^{-1}$.

Taking the logarithm of both sides of formula (1) leads to

$$\ln \dot{\varepsilon} = \ln A - \left(\frac{Q}{RT}\right) + n \ln[\sin h(\alpha\sigma)], \tag{8}$$

$$Q = R\left(\frac{\partial \ln[\sin h(\alpha\sigma)]}{\partial(1/T)}\Big|_{\dot{\varepsilon}}\right)\left(\frac{\partial \ln \dot{\varepsilon}}{\partial \ln[\sin h(\alpha\sigma)]}\Big|_{T}\right) = RKH, \tag{9}$$

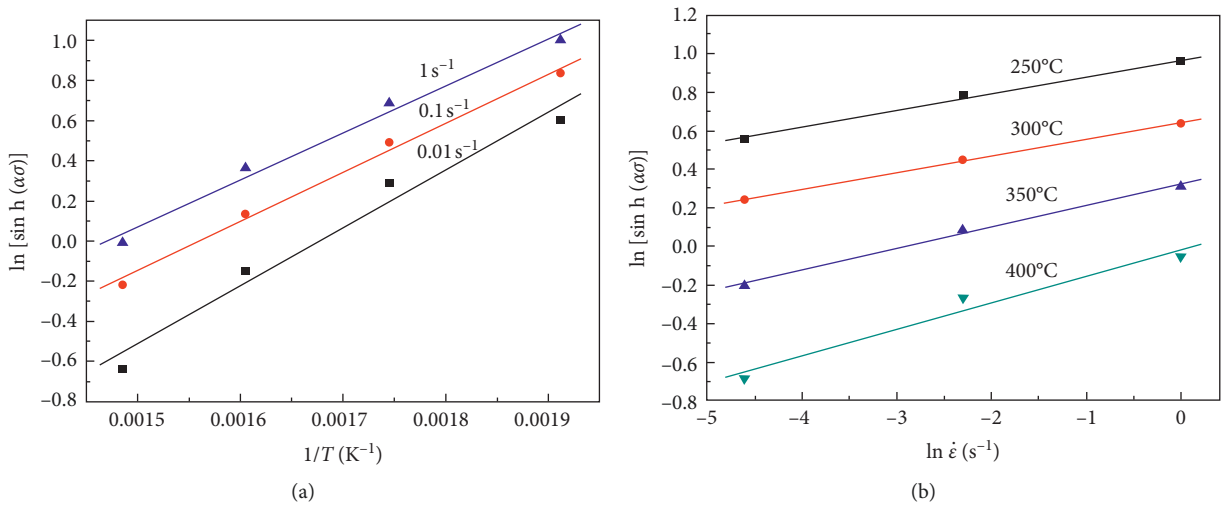

FIGURE 3: Curves of peak stress versus strain-rate and temperature under different conditions: (a) $\ln[\sin h(\alpha\sigma)] - (1/T)$; (b) $\ln\dot{\varepsilon} - \ln[\sin h(\alpha\sigma)]$.

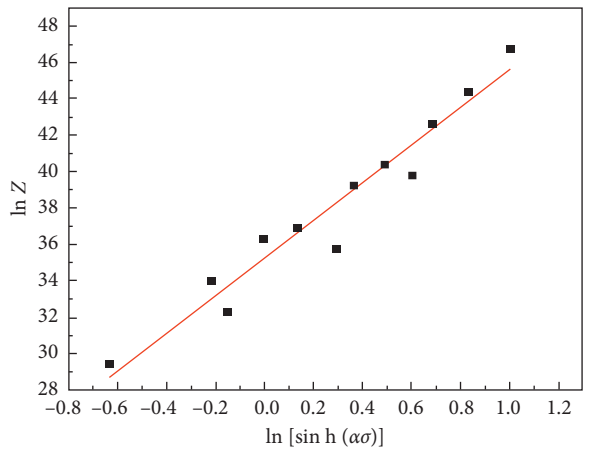

FIGURE 4: Curve of $\ln Z - \ln[\sin h(\alpha\sigma)]$.

where K and H are expressed as the linear slopes of $\ln[\sin h(\alpha\sigma)] - (1/T)$ and $\ln\dot{\varepsilon} - \ln[\sin h(\alpha\sigma)]$, respectively.

The peak stress values under different conditions were regarded as strain-stress, and the relationship curves of $\ln[\sin h(\alpha\sigma)] - (1/T)$ and $\ln\dot{\varepsilon} - \ln[\sin h(\alpha\sigma)]$ were fitted, as showed Figure 3.

The linear slope reciprocal of the mean value was obtained, and these values were substituted into formula (9). Accordingly the hot deformation activation energy (Q) was obtained, that is, $Q = 203107.713$J/mol.

Zener et al. [20, 21] discovered that material deformation conditions (deformation temperature, strain rate, etc.) directly affect the true stress-strain, so they introduced the parameter Z. Taking the logarithm of both sides of formula (10) leads to

$$Z = \dot{\varepsilon}\exp\left(\frac{Q}{RT}\right) = A[\sin h(\alpha\sigma)]^n, \tag{10}$$

$$\ln Z = n\ln[\sin h(\alpha\sigma)] + \ln A. \tag{11}$$

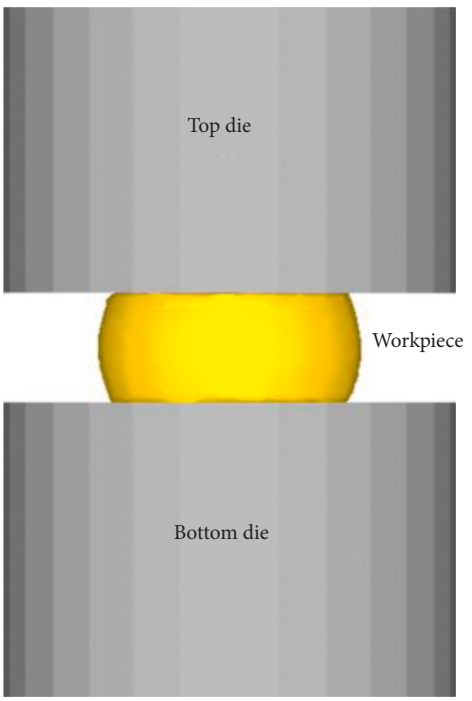

FIGURE 5: Material deformation diagram at plastic pressure.

Based on formula (11), the data of $\ln Z - \ln[\sin h(\alpha\sigma)]$ were fitted as shown in Figure 4, and n and $\ln A$ were obtained, that is, $n = 10.228$ and $\ln A = 35.243$.

Finally, experimental data were fitted, and the high-temperature constitutive model was obtained as follows:

$$\dot{\varepsilon} = 2.424 \times 10^{15}[\sin h(0.0111\sigma)]^{10.228} \times \exp[-203107.713(8.314T)]. \tag{12}$$

Then, this model was inputted into user-defined materials' database in FEM software for further numerical computation.

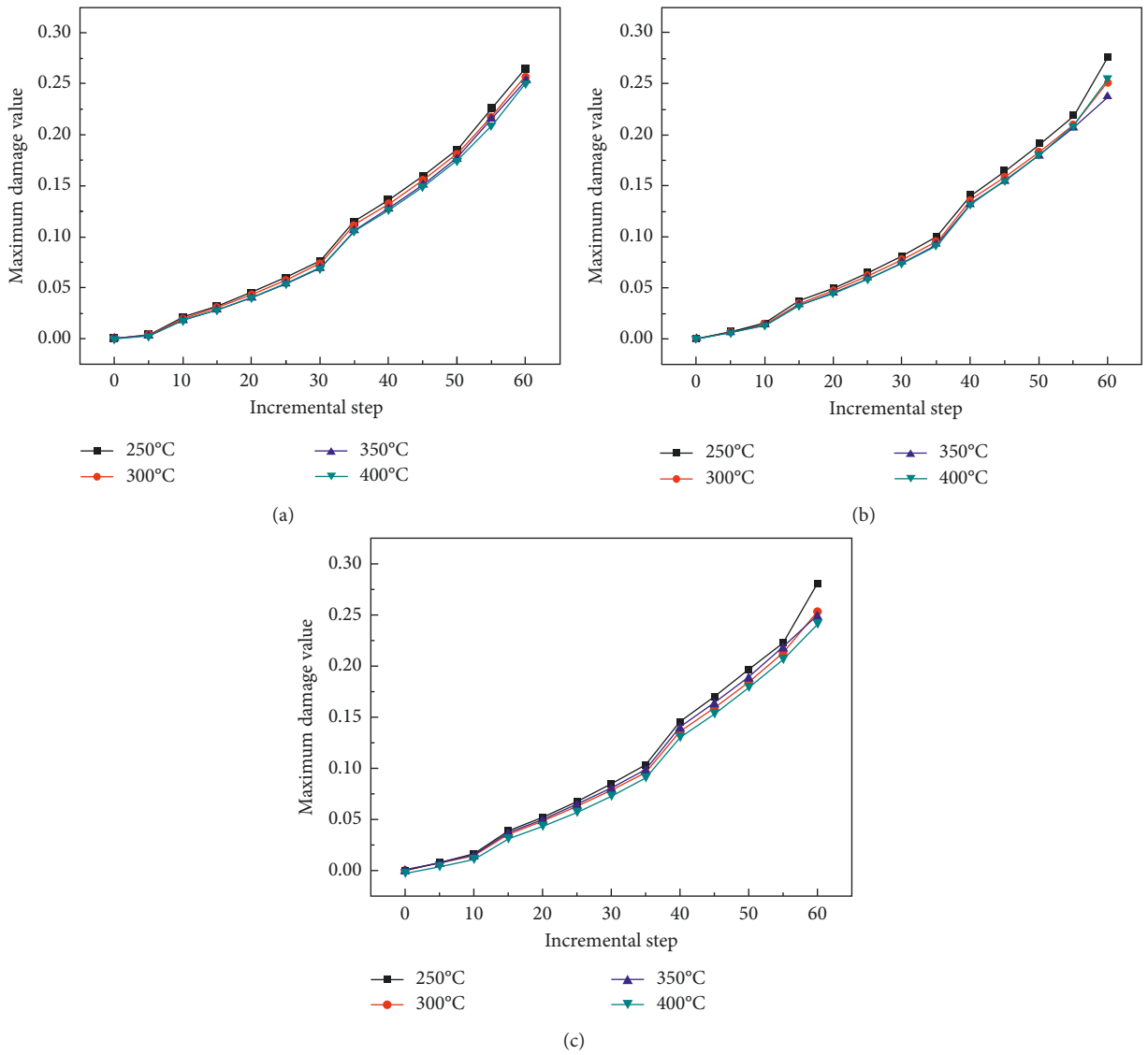

FIGURE 6: Damage variation on the outer edge of the upsetting drum at different temperatures and strain rates. (a) $\dot{\varepsilon} = 0.01\text{s}^{-1}$; (b) $\dot{\varepsilon} = 0.1\text{s}^{-1}$; (c) $\dot{\varepsilon} = 1\text{s}^{-1}$.

3.2. Critical Damage Factor. Ductile damage fracture is a very complicated process closely related to process and material parameters. Cockcroft and Latham [18] have put forward a criterion through a dimensionless stress concentration factor, which generalizes unit volume plastic work. The equation is as follows:

$$\int_0^E \frac{\overline{\sigma}}{\sigma} \cdot d\varepsilon = C_1, \tag{13}$$

where σ, $d\varepsilon$, ε, and $\overline{\sigma}$ are the equivalent stress, equivalent plastic-strain increment, crack equivalent strain, and maximum tensile strain, respectively. C_1 is a material constant. Cockcroft and Latham thought that C_1 is an important indicator to measure material failure, and its limit value C_1 is the critical damage factor.

Other researchers have put forward the notion of the critical damage factor [22]. The ratio between the unit time increment of the damage incremental and existing cumulative damage quantity is expressed as

$$m_{\text{dam}} = \frac{\Delta A}{A_{\text{accum}}}, \tag{14}$$

where m_{dam}, ΔA, and A_{accum} are the damage sensitive rate, unit time damage incremental, and existing cumulative damage quantity, respectively.

3.2.1. Numerical Simulation of Thermal Compression Test. Material true stress-strain curves under different temperatures and Arrhenius constitutive model were inputted into material library of the Finite Element Program DEFORM to simulate the hot compression test. The diagram of deformation under plastic pressure is shown in Figure 5. In order to simulate the thermal simulation experiment, the

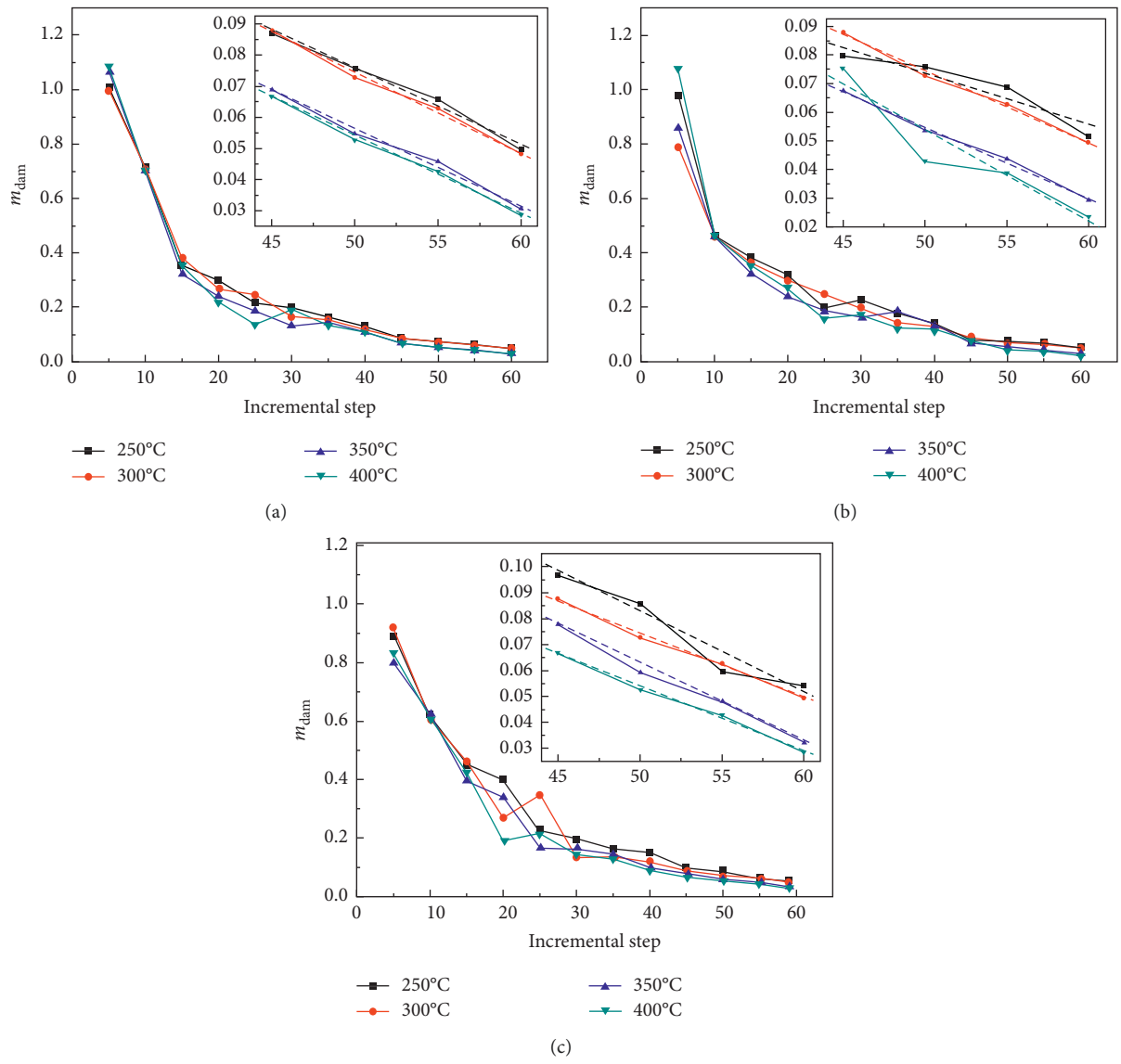

FIGURE 7: Variation in the damage sensitive rate on the outer edge of the upsetting drum at different temperatures and strain rates. Greater details of the graphs from (a)–(c) above 40 increment steps are shown in insets. (a) $\dot{\varepsilon} = 0.01\text{s}^{-1}$; (b) $\dot{\varepsilon} = 0.1\text{s}^{-1}$; (c) $\dot{\varepsilon} = 1\text{s}^{-1}$.

damage distributions of the magnesium alloy at different temperatures and different strain rates were analyzed, and the relationships between strain rate and temperature and damage factor were further studied.

3.2.2. Cockcroft–Latham of the Critical Damage Factor and Damage Sensitive Rate. The result shows that the minimum damage value always appears in the billet central zone, while the maximum damage value always appears on the outer edge of the upsetting drum. The distribution regularities of the outer drum are shown in Figure 6. Distribution regularities of the maximum damage value are not obvious, and the curves are very close to each other under different temperatures at a strain rate of 0.01 s^{-1}. However, distributions of the damage value become fluctuated at strain rates of 0.1 s^{-1} and 1 s^{-1}, and the maximum damage values decrease when temperature gets higher at these two strain rates. This phenomenon is called damage softening, which is more sensitive to strain rate.

The outer edge of the upsetting drum is also regarded as the research object. The ratio between unit time increment of the damage incremental and existing cumulative damage quantity is shown in Figure 7. It is found that damage sensitive rate always decreases quickly in the first 5 s, and the damage sensitive rate fluctuates between 0.5 s and 1.5 s until it approaches zero.

Damage sensitive rate curves are also amplified locally in Figure 7. And in this amplified figures, local curves do not approach zero under different strain rates of 0.01 s^{-1}, 0.1 s^{-1}, and 1 s^{-1}. But local curves should be fitted to reach zero in order to reveal the compression step of the damage sensitive rate. Meanwhile, existing cumulative damage values are determined by numerical simulation results, and these

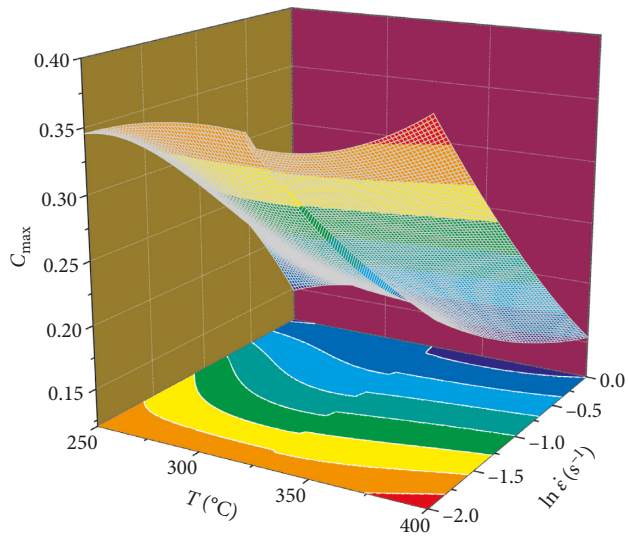

FIGURE 8: Temperature and strain rate effect on the critical damage value of AZ31 magnesium alloy.

values are the critical damage factor. According to this method, distribution regularities of the damage value are determined at different temperatures and strain rates (Figure 8). The critical damage factor is found to be inconstant and varies from 0.1445 to 0.3759.

The critical damage factor will decrease obviously with the increasing of strain rate at the same temperature. Critical damage factor will change little with the increasing of temperature at the same strain rate.

4. Conclusions

In this paper, AZ31 was regarded as the research object. True stress-strain curves were obtained by the high-temperature tensile test. Based on these experimental data, some parameters were solved, and a high-temperature constitutive model was constructed. The Arrhenius constitutive model was inputted into material library of the Finite Element Program DEFORM. Simulation accuracy is substantially improved by the constitutive equation. Then, a hot compression test simulation is proceeded. Finally, critical damage values were obtained at temperatures between 250°C and 400°C and strain rates between 0.01 s^{-1} and 1 s^{-1}. The maximum damage value always appears at the outer edge of the upsetting drum. Distribution regularities of the maximum damage value regularly increases with increased temperature at a strain rate of 0.01 s^{-1}. However, distribution regularities of the damage value are poor at a strain rate of 0.1 s^{-1} and 1 s^{-1}. Distribution regularities of the damage values are determined at different temperatures and strain rates. The critical damage factor is not a constant and fluctuates from 0.1445 to 0.3759.

Conflicts of Interest

The authors declare that there are no conflicts of interest regarding the publication of this paper.

Acknowledgments

The authors thank the National Natural Science Foundation of Guangdong Province (no. 2017A030310621) for financial support of this research.

References

[1] S. A. Sani, G. R. Ebrahimi, and A. R. K. Rashid, "Hot deformation behavior and dynamic recrystallization kinetics of AZ61 and AZ61+Sr magnesium alloy," *Journal of Magnesium and Alloys*, vol. 4, no. 2, pp. 104–114, 2016.

[2] Y. Xue, Z. M. Zhang, and Y. J. Wu, "Study on critical damage factor and constitutive model including dynamic recrystallization softening of AZ80 magnesium alloy," *Science of Sintering*, vol. 45, no. 2, pp. 199–208, 2013.

[3] J. Luan, C. Sun, X. Li, and Q. Zhang, "Constitutive model for AZ31 magnesium alloy based on isothermal compression test," *Materials Science and Technology*, vol. 30, no. 2, pp. 211–219, 2014.

[4] K. K. Alaneme and E. A. Okotete, "Enhancing plastic deformability of Mg and its alloys: a review of traditional and nascent developments," *Journal of Magnesium and Alloys*, vol. 5, no. 4, pp. 460–475, 2017.

[5] P. Monica, P. M. Bravo, and D. Cardenas, "Deep cryogenic treatment of HPDC AZ91 magnesium alloys prior to aging and its influence on alloy microstructure and mechanical properties," *Journal of Materials Processing Technology*, vol. 239, pp. 297–302, 2017.

[6] X. Liu, L. X. Li, and B. W. Zhu, "Modeling of the flow stress behavior and microstructural evolution during hot deformation of Mg–8Al–1.5Ca–0.2Sr magnesium alloy," *Journal of Magnesium and Alloys*, vol. 2, no. 2, pp. 133–139, 2014.

[7] J. Lee, S. J. Kim, Y. S. Lee, J. Y. Lee, D. Kim, and M. G. Lee, "Distortional hardening concept for modeling anisotropic/asymmetric plastic behavior of AZ31B magnesium alloy sheets," *International Journal of Plasticity*, vol. 94, pp. 74–79, 2017.

[8] M. Ambati, R. Kruse, and L. D. Lorenzis, "A phase-field model for ductile fracture at finite strains and its experimental verification," *Computational Mechanics*, vol. 57, no. 1, pp. 149–156, 2016.

[9] M. Ambati, T. Gerasimov, and L. D. Lorenzis, "Phase-field modeling of ductile fracture," *Computational Mechanics*, vol. 55, no. 5, pp. 1017–1040, 2015.

[10] R. Luri, J. P. Fuertes, C. J. Luis, D. Salcedo, I. Puertas, and J. Leon, "Experimental modeling of critical damage obtained in Al–Mg and Al–Mn alloys for both annealed state and previously deformed by ECAP," *Materials and Design*, vol. 90, pp. 881–890, 2016.

[11] Y. Tong, Z. Q. Guo, and B. Chen, "A constitutive description for drawing limit of magnesium alloy tube based on continuum damage mechanics," *Materials Science Forum*, vol. 610–613, pp. 951–954, 2009.

[12] R. Kawalla, U. Prahl, M. Moses, H. Wemme, J. Luft, and M. Kirschner, "Improvement of manufacturing technology for thin-walled pipes made of copper alloys," *Materials Science Forum*, vol. 918, pp. 140–144, 2018.

[13] F. Lambiase and A. D. Llio, "Damage analysis in mechanical clinching: experimental and numerical study," *Journal of Materials Processing Technology*, vol. 230, pp. 109–120, 2016.

[14] M. C. Kaye, D. Balint, J. Lin, and D. Farrugia, "Test-piece design for experimental and numerical evaluation of damage in relation to spatial triaxial stress inversion," *International*

Journal of Damage Mechanics, vol. 26, no. 4, pp. 588–607, 2017.

[15] X. H. Hu, K. S. Choi, X. Sun, and S. F. Golovashchenko, "Edge fracture prediction of traditional and advanced trimming processes for AA6111-T4 sheets," *Journal of Manufacturing Science and Engineering*, vol. 136, no. 2, pp. 021016–021026, 2014.

[16] L. B. Yang, H. Zhang, and D. S. Peng, "Study of mechanic behavior for 7075 aluminum alloy under hot-working conditions," *Hot Working Technology*, vol. 31, no. 1, pp. 1–5, 2002.

[17] H. Wu, S. P. Wen, H. Huang et al., "Hot deformation behavior and constitutive equation of a new type Al–Zn–Mg–Er–Zr alloy during isothermal compression," *Materials Science and Engineering: A*, vol. 651, no. 10, pp. 415–424, 2016.

[18] M. G. Cockcroft and D. J. Latham, "Ductility and the workability of metals," *International Journal of Minerals, Metallurgy, and Materials*, vol. 96, no. 6, pp. 33–39, 1968.

[19] Y. Y. Dong, C. S. Zhang, G. Q. Zhao, Y. J. Guan, A. J. Gao, and W. C. Sun, "Constitutive equation and processing maps of an Al–Mg–Si aluminum alloy: determination and application in simulating extrusion process of complex profiles," *Materials and Design*, vol. 92, no. 15, pp. 983–997, 2016.

[20] C. Zener and J. H. Hollomon, "Effect of Strain Rate on the Plastic Flow of Steel," *Journal of Applied Physics*, vol. 15, no. 1, pp. 22–32, 1994.

[21] X. Liang, "Damage accumulation and fracture initiation in uncracked ductile solids subject to triaxial loading," *International Journal of solids and Structures*, vol. 44, no. 16, pp. 5163–5181, 2007.

[22] Q. G. Zheng, Y. X. Wang, Y. W. Zhang, and F. B. Wang, "Effect of different temperatures and strain rates on the critical damage factor of 7075 aluminum alloy," *Journal of Chongqing University*, vol. 34, no. 7, pp. 51–56, 2011.